Chapter 5

Ghost diffraction

5.1 Introduction

Image recovery elicited from the correlation of a stochastic light has been the subject of significant research interests in the classical and quantum domains [67, 195, 196]. Over the past few years, a plethora of attention has been shown to recover the image using the intensity correlation between two light fields, and techniques such as ghost diffraction (GD) and ghost imaging (GI) have emerged [197, 198, 199, 200]. Compared to conventional imaging techniques, the GD and GI uses a non-spatially resolved bucket detector to collect light originating from a transparency either in reflection or transmission geometry. In these techniques, one light field interacts with the transparency and detected by a bucket detector. The second light field which does not interact with the object, directly propagates to the spatially resolved detector having array of pixels. A spatial structure and diffraction pattern of the transparency image can be retrieved by correlating the information measured by the bucket with the information recorded by the array detector in the second arm which never interacts with the transparency. The GD and GI were initially demonstrated with the entangled photons generated in spontaneous parametric down-conversion [201, 202]. It was demonstrated later that quantum entangled sources are not necessary and realizations

of GD and GI are also possible with the classical correlated light [203] as well as thermal light [204, 205]. Since then, significant attention has been attributed to these techniques with classical light for applications in remote sensing [206] , biomedical optics [207] , microscopy [208] , temporal imaging [209] , averaged speckle patterns [210] etc. Another important trend in the GD and GI makes use of digital insertion of the random phase masks in the coherent light to realize computational imaging [211, 212, 213]. However, major interests in the GD and GI are limited to recovery of only the modulus square of the Fourier spectrum [205, 214, 215] , without a phase recovery except for some investigations. A modified Young's interferometer was employed to measure the field correlation in the GD and to recover the phase information [216]. A few ghost schemes have also been developed with specific attention to phase recovery [217, 218, 219]. Recently, phase recovery in the GD has been demonstrated using the interference of coherent waves using the spatially fluctuating field. This technique uses a combination of Mach-Zehnder interferometers, i.e., inner and outer interferometer assembly [172]. Experimental implementations on the GD and GI usually employ rotating ground glass (RGG) to mimic a pseudo thermal light source. Such experimental implementation uses temporal averaging as a substitute for ensemble averaging on the premise of temporal stationarity and temporal ergodicity. On the other hand, a spatial statistical regime is equally important and needs attention in a situation where temporal averaging is not possible. For instance, spatial statistics of the randomly scattered coherent field, such as laser speckle, provide useful statistical information. Moreover, it permits the replacement of the ensemble average by the spatial average under consideration of spatial stationarity and spatial ergodicity [122] . In spite of its practical importance and common occurrence, spatial fluctuations of laser speckles appear to have not attracted attention in the GD and GI except a recent investigation [172] . To fill this gap and explore use of the spatial ergodicity, we propose and demonstrate the GD scheme with a static ground glass (SGG) rather than RGG. The idea is to examine the reconstruction

of a transparency image using basic principle of the GD with the spatial statistical optics approach. Moreover, a phase retrieval algorithm is combined with the results of the GD to retrieve transmission function of a planar object. This iterative algorithm together with digital processing operations overcomes the phase loss issue. This strategy helps to recover the transparency information using spatial intensity correlation between the random fields from a single pixel of a detector and array of pixels without object in the GD scheme. Here, single pixel in our scheme refers use of only one pixel intensity of the random light coming from the object arm. This single pixel of a detector at the observation plane is a replacement of the single pixel detector used in the GD. Experimental tests of the proposed scheme is carried out, and experimental results are compared with simulation results. A good agreement between the experiment and simulation supports the use of a new reconstruction approach in the correlation based imaging, and spatial statistical optics approach for Ghost Diffraction studies. Moreover, a quantitative analysis of retrieved results is provided by utilizing the visibility and reconstruction efficiency parameters. The detailed theoretical explanation, method, corresponding experimental and simulation results are presented below.

5.2 Methodology

A comparison of the GD setup with RGG, and our experimental geometry of the proposed technique with the SGG is shown in Fig. 5.1. Usually, the RGG generates temporally fluctuating speckle patterns for realization of the ensemble averaging as shown in Fig. 5.1(a). Here, we present realization of the ensemble average by the spatial averaging [122] , and two replicas of the speckle pattern are utilized. Therefore, RGG is replaced by a static ground glass (SGG) as shown in Fig. 5.1 (b). Consider two identical copies of the light field distribution at a source plane, say $z = 0$. Let $E(\rho)$ denote the optical field at a particular instant of time, i.e., a single realization of the RGG. A beam splitter (BS)

is used to create two copies of the optical field. Furthermore, at the plane $z = 0$, one of the two copies illuminates the transparency $\tau(\rho)$ and propagates to the observation plane. Consider the propagation of a monochromatic light field from source plane to observation plane at a distance $z = d$ in the Ghost diffraction (GD) scheme. The instantaneous light fields reaching at the observation plane are represented as,

$$E_1(r) = \int \tau(\rho) E_1(\rho) G(r-\rho) d\rho \tag{5.1}$$

$$E_2(r) = \int E_2(\rho) G(r-\rho) d\rho \tag{5.2}$$

where ρ and r are the spatial coordinates at source plane and observation plane respectively. $E_1(r)$ is the light field at detector plane with the transparency $\tau(\rho)$ and $E_2(r)$ is the light field reaching at the observation plane without carrying transparency as desired in the GD. The term $G(r,\rho)$ denotes the propagation kernel, which is represented as,

$$G(r,\rho) = \frac{exp(ikz)}{i\lambda z} exp(ik\frac{|r|^2 + |\rho|^2 - 2r.\rho}{2z}) \tag{5.3}$$

where $k = \frac{2\pi}{\lambda}$ and λ are the wave number and wavelength of light, respectively. Propagation distance is denoted by z. Therefore, the light field at the observation plane is given as,

$$E_1(r) = \frac{exp(ikz)}{i\lambda z} exp(ik\frac{|r|^2}{2z}) \iint exp(ik\frac{|\rho_1|^2 - 2r.\rho_1}{2z}) E_1(\rho_1)\tau(\rho_1) d\rho_1 \tag{5.4}$$

$$E_2(r) = \frac{exp(ikz)}{i\lambda z} exp(ik\frac{|r|^2}{2z}) \iint exp(ik\frac{|\rho_2|^2 - 2r.\rho_2}{2z}) E_2(\rho_1) d\rho_2 \tag{5.5}$$

The transparency information is encoded into the spatial correlation functions of the intensities $\langle I_1(r_1) I_2(r_2) \rangle$ .The intensities in two different arms of the GD scheme are

represented as,

$$I_1(r_1) = E_1^*(r_1)E_1(r_1) \tag{5.6}$$

$$I_2(r_1) = E_2^*(r_2)E_2(r_2) \tag{5.7}$$

A correlation of intensity fluctuation of these two spatially fluctuating light fields is represented as,

$$g^2(r_1,r_2) = \langle \Delta I_1(r_1)\Delta I_2(r_2)\rangle = \langle I_1(r_1)I_2(r_2)\rangle - \langle I_1(r_1)\rangle\langle I_2(r_2)\rangle \tag{5.8}$$

where, $\Delta I_p(r) = I_p(r) - \langle I_p(r)\rangle$ is the fluctuation of intensity at a location r over its mean value, and $< ... >$ represents the ensemble average. Using Eq. (5.6), (5.7) and substituting Eq. (5.4) and (5.5) into Eq. (5.8) results into cancellation of the phase curvature outside the integral $\frac{exp(ikz)}{i\lambda z} exp(ik\frac{|r|^2}{2z})$ and this helps to get the spatial ergodicity and spatial stationarity at the observation plane. Moreover, correlation of intensity fluctuations can be expressed as modulus square of the two-point field correlation as,

$$g^2(r_1,r_2) = |\langle E_1^*(r)E_2(r+\Delta r)\rangle|^2 \tag{5.9}$$

For further calculations, let us consider a change of variables, $r_2 = r+\Delta r$ and $r_1 = r$. The field correlation can be extracted by applying the spatial averaging as a replacement of the ensemble averaging,

$$\langle E_1^*(r)E_2(r+\Delta r)\rangle = \iiint E_1^*(\rho_1)E_2(\rho_2)exp(\tfrac{-ik(|r_1|^2)-|r_2|^2}{2z})exp(\tfrac{-ik((r+\Delta r).\rho_2)-r.\rho_1)}{2z})d\rho_1 d\rho_2 dr$$

$$= \iint E_1^*(\rho_1)\tau(\rho_1)E_2(\rho_2)exp(\tfrac{-ik(|r_1|^2)-|r_2|^2}{2z})exp(\tfrac{-ik(\Delta r.\rho_2}{z})exp(\tfrac{-ik(\rho_2-\rho_1).r}{z}dr)d\rho_1 d\rho_2 \tag{5.10}$$

Here, we employ the following equation using space averaging under the condition of spatial stationarity and ergodicity and follows the same analogy as used in temporal averaging. Therefore, ensemble average is supplanted by space averaging instead of time averaging.

$$\int exp(\frac{-ik((\rho_2-\rho_1).r)}{z})dr = \delta(\rho_2-\rho_1) \tag{5.11}$$

Therefore, Eq. (5.10) takes the form of,

$$\langle E_1^*(r)E_2(r+\Delta r)\rangle = \int I(\rho)\tau(\rho)exp(\frac{-i2\pi\Delta r.\rho}{\lambda z})d\rho \tag{5.12}$$

$$\langle E_1^*(r)E_2(r+\Delta r)\rangle \propto \int \tau(\rho)exp(\frac{-i2\pi\Delta r.\rho}{\lambda z})d\rho \tag{5.13}$$

where, we have considered $\rho_1 = \rho$ and Eq. (5.13) is considered under assumption of uniform illumination intensity at the source, i.e. $I(\rho) = 1$. Utilizing the spatial stationarity at the observation plane and considering $r_2 = r+\Delta r$ and $r_1 = r$, the correlation of the intensity fluctuations can now be represented as,

$$g^2(\Delta r) = |F(\Delta r)|^2 \tag{5.14}$$

where $|F(\Delta r)|$ is the amplitude of Fourier transform of transparency $\tau(\rho)$. Eq. (5.14) states that the correlation between intensity fluctuations reconstructs the amplitude of the Fourier spectrum of the transparency. Moreover, Fourier spectrum depends only on the difference between two coordinates, i.e., $r_2 - r_1$. The spatial distribution of the Fourier spectrum is obtained by spatially varying the detection point in the reference arm and keeping the detection position of the transparency arm at $r_1 = 0$. However, the phase distribution of the Fourier spectrum is lost in Eq. (5.14) and this obstructs recovery of the transparency $\tau(\rho)$.

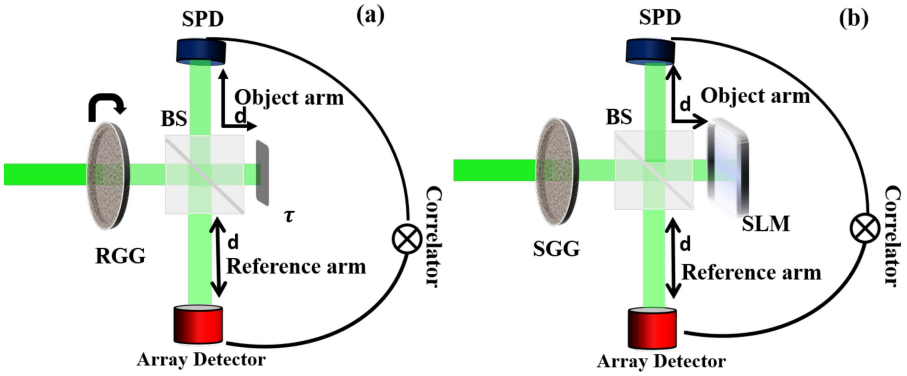

Fig. 5.1 Conceptual representations of a GD scheme with RGG and our proposed GD scheme (a) ghost diffraction scheme with RGG: rotating ground glass, SPD: Single Pixel Detector, transparency- τ, reflective type. (b) Proposed ghost diffraction scheme with SGG: Static Ground Glass, BS: Beam Splitter

To overcome this issue, we make use of a phase retrieval algorithm; Fienup type algorithm [187, 220, 221] by using few constraints. This helps to resolve the phase loss problem in the intensity correlation measurement. The correlation of the intensity fluctuations obtained in Eq. (5.14) is subjected to the phase retrieval algorithm with the constraint that the $\tau(\rho)$ is real and positive. Additionally, we also applied a loose support constraint (the support is the set of points over which the object function is nonzero). Prior to using the phase retrieval approach, the noisy regions of the intensity correlation function were removed from the observed far field using a 2D Tucky window. A hybrid input–output (HIO) algorithm with a fixed β value is used to implement the phase retrieval algorithm, where β is the feedback parameter that controls the convergence properties of the HIO algorithm. Moreover, the residual noise from the retrieved image is reduced using an error-reduction method [187] . A flow chart for the understanding of implementation of the phase retrieval algorithm is given in Fig. 5.2.

The algorithm starts with an initial guess of transparency $\tau(\rho)$, which is fed to the process as mentioned in Fig. 5.2. Amplitude of the Fourier spectrum obtained in Eq. (5.14) is fed to the algorithm and process goes on for p^{th} iterations. By applying the constraints

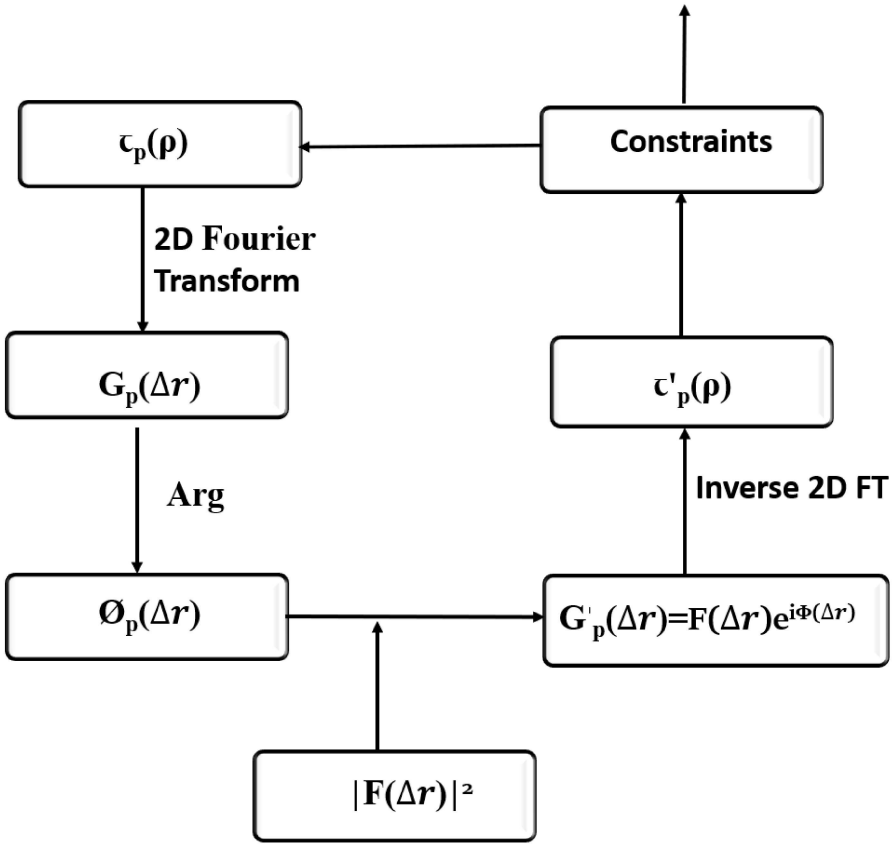

Fig. 5.2 Block diagram for the phase retrieval algorithm

to the transparency that it should be real and non-negative, the output of the p^{th} iteration, $\tau_p^{'}(\rho)$ is used as an input for the next $(p+1)^{th}$ iteration. Now few iterations of hybrid input output algorithm (HIO) are implemented as following.

$$\tau_{p+1}(\rho) = \left\{ \begin{array}{ll} \tau_p^{'}(rho) & for\ \rho \notin S \\ \tau_p(rho) - \beta\tau_p^{'}(rho) & for\ \rho \in S \end{array} \right\} \tag{5.15}$$

Further the output of HIO algorithm is applied to an error reduction algorithm which is described as below.

$$\tau_{p+1}(\rho) = \left\{ \begin{array}{ll} \tau_p^{'}(rho) & for\ \rho \notin S \\ 0 & for\ \rho \in S \end{array} \right\} \tag{5.16}$$

S is the set of all points on $\tau_p^{'}(\rho)$ that does not follow the constraints. Several iterations were performed and different values of β were used for the faithful reconstruction with a good convergence. Thus, with help of the mentioned algorithm, the transparency function is retrieved from the amplitude variation of the Fourier spectrum of transparency obtained in Eq. (5.14). To demonstrate the proposed technique, we simulate the experimental scheme as shown in Fig. 5.1(b) and confirm it experimentally.

5.3 Experiment

The experimental setup of the proposed technique is shown in Fig. 5.3. A monochromatic

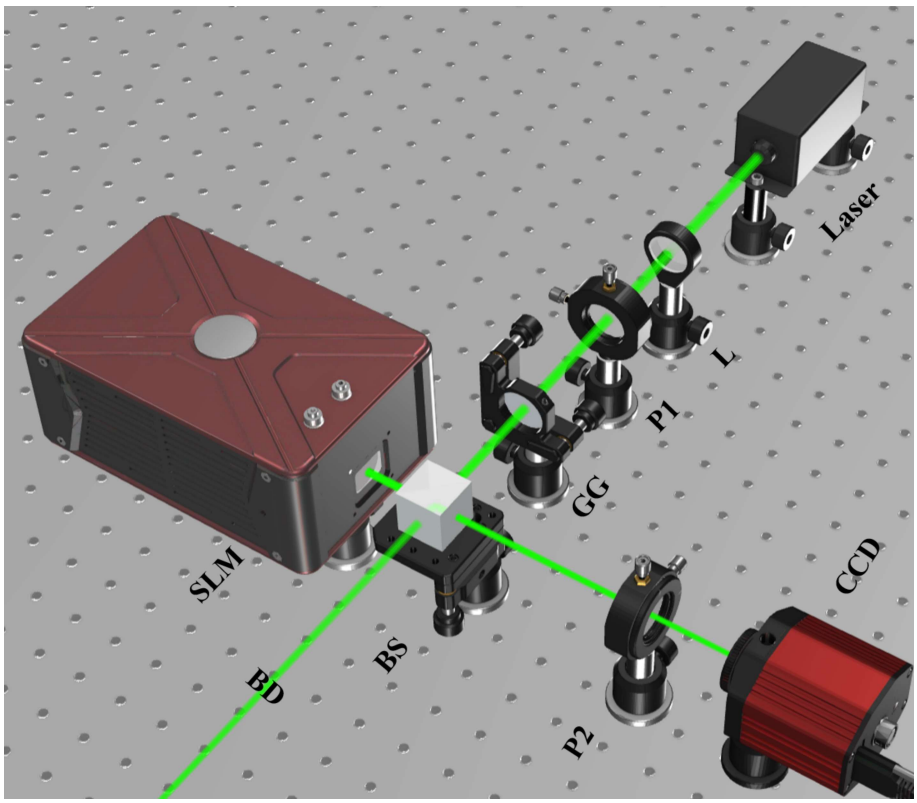

Fig. 5.3 Schematic of the experimental setup of the proposed technique, L: lens, $P_n(n=1,2)$: Polarizers, GG: Ground glass, SLM: Spatial Light Modulator, BS: Beam splitter, CCD: Charge-Coupled device. BD-Beam Dumped.

laser beam (532 nm) is spatially filtered and collimated with the help of a collimating lens (L). This collimated beam of diameter 4.8 mm illuminates a SGG, and the randomly scattered field splits into two parts by a BS. The light transmitted from the BS is dumped. The reflected beam goes to a spatial light modulator TNLC-SLM (LCR720 model manufactured by HOLOEYE) to insert transparency $\tau(\rho)$ into the light. The beam reflected from SLM goes back to the BS; and travels to a detector where we use only a single pixel of the detector for a selected patch of the intensity. A polarizer (P) with axis horizontal, is placed right before the detector to make the uniform polarization in the recorded speckle pattern. The detection plane is located at a distance $d = 150mm$ from the SLM. In the second case, the SLM is switched off and the speckle pattern reflected by the SLM travels back to the detector plane and is recorded by an array of pixels of the charged coupled device (CCD). The CCD camera has a pixel resolution of 2200×2752 and pixel size 4.54 μm (Procilica, GT-2750). Detailed procedure to evaluate the spatial intensity correlation in the GD scheme with the spatial statistical optics is explained in Fig. 5.4. A random field reflected by the transparency is recorded by detector and only a single pixel data of the intensity patch is used as shown in Fig. 5.4(a). On the other hand, the second random field is recorded by array of pixels with the SLM off condition, i.e., without any transparency function, and an intensity patch composed of arrays of pixels as shown in Fig. 5.4(b). Therefore, stage of ensemble averaging is shifted from the rotating diffuser to the positional scanning of the spatially fluctuating random fields at the observation plane as highlighted by arrows in Figs. 5.4(a) and 5.4(b), 5.4(d) and 5.4(e).

5.4 Results and Discussion

Taking a portion of the speckle pattern as a matrix $I_p(r_x, r_y)$ which represents one realization of the randomly scattered field as shown in Fig. 5.4. Here x and y are pixel spatial coordinates and may take values up to 300×300 pixels. For the field with transparency,

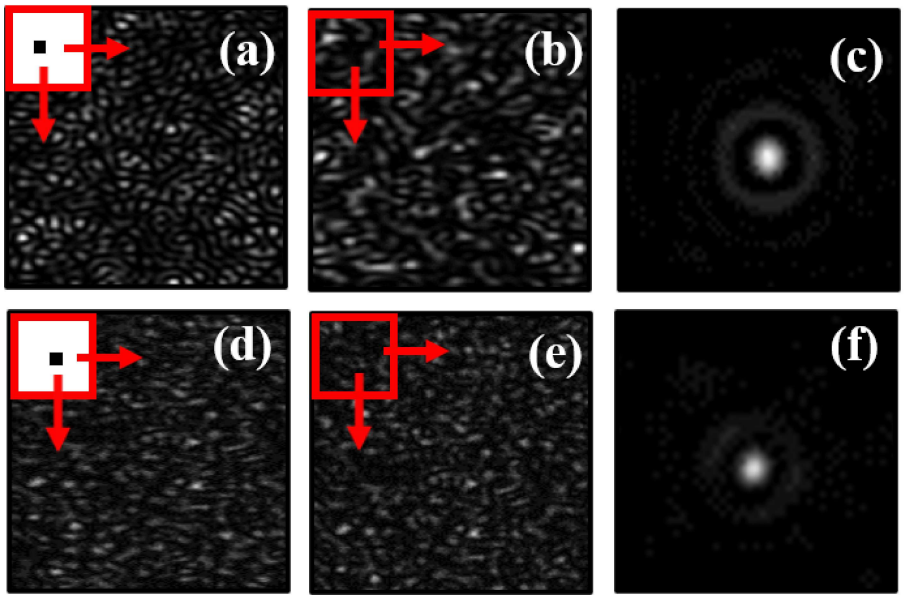

Fig. 5.4 Simulation Study (a-c): (a) only a single pixel of random field with transparency and scanning of single pixel in the space (b) window of the reference speckle and its scanning (c) Far-field pattern for annular aperture by simulation; Experimental Study (d-f): (d) only a single pixel of random field with transparency and scanning of single pixel in the space (e) window of the reference speckle and its scanning (f) Far-field pattern for annular aperture by experiment

we select only a central single pixel out of the 300 $\times$ 300 window, i.e., pixel (151,151) as shown in Figs. 5.4(a) and 5.4(d). The array of pixels 300 $\times$ 300 presents speckle without transparency as shown in Figs. 5.4(b) and 5.4(e). A small black square in the center of big red square represents only one pixel of the 300 $\times$ 300 window of object's random field in Figs. 5.4(a) and 5.4(d). This single pixel mimics the single pixel detector used in conventional GD schemes. The big red square in Figs. 5.4(b) and 5.4(e) represents the 300 $\times$ 300 window of random field without any object information. The single pixel of object speckle is correlated with the 300 $\times$ 300 pixels window of speckle without any object information. The red arrows represent that it is scanned over entire recorded speckle pattern of size 1000 $\times$ 1000 pixels. The cross-covariance of the intensity pattern is obtained by correlating $\Delta I_1(0,0)\Delta I_2(r_x,r_y)$ for different scanning positions as marked in Figs. 5.4(a), 5.4(b), 5.4(d) and 5.4(e), and the process of scanning is represented as

$\sum_{m=1}^{M} \frac{\Delta I_1^m(0,0)\Delta I_2^m(r_x,r_y)}{M}$. Here M represents number of different windows of the matrix $I_p^m(r_x,r_y)$ and produced by the pixel-by-pixel movement of the matrix $I_p(r_x,r_y)$ over the speckle. We have used a speckle pattern of size 1000×1000 pixels and 2D scanning of $I_p(r_x,r_y)$ over the speckle patterns provide 700×700 different realizations. The spatial intensity correlation results for simulation and experiment for a transparency, i.e., an annular aperture (size 2.8 mm), are presented in Figs. 5.4(c) and 5.4(f) respectively. A random field is recorded at d, and intensity correlation permits realization of a lensless Fourier transform even in the Fresnel domain. Simulation of the experimental situation is implemented under consideration of following steps: propagation of coherent light with transparency through a diffuser with random phase uniformly distributed between $[-\pi,\pi]$, use of the angular spectrum method for propagation. Subsequently, these simulated random intensities are used to evaluate cross-covariance of the intensities as defined in Eq. (5.13). For simulation, we evaluate the Fourier pattern from the cross-correlation of intensity fluctuations as described earlier. A phase retrieval algorithm is applied to the far-field pattern to reconstruct the transparency. Furthermore, the recovery of two different transparencies, namely annular ring and sinusoidal grating, from the intensity correlation is demonstrated. Starting from crystallography to optics, the idea of phase recovery from the Fourier intensity has been explored widely. By applying appropriate constraints in the respective domains, iterative phase retrieval methods work by switching back and forth between object and Fourier space. The constraints are additional a priori information about the object which help in the unique phase reconstruction.Here we implement a phase retrieval algorithm (Fienup-type algorithm) is applied to the far-field pattern(Fourier intensity), using constraints that the $\tau(\rho)$ is real and positive. Moreover, we have also used a loose support constraint (the support is the set of points over which the object function is nonzero). Before applying the phase retrieval algorithm, a 2D Tucky window was used on the measured far field, to remove the noisy sections in intensity correlation function. A

standard version of the phase retrieval algorithm is implemented in MATLAB software consisting of a hybrid input–output (HIO) algorithm with a fixed β value. An Error-

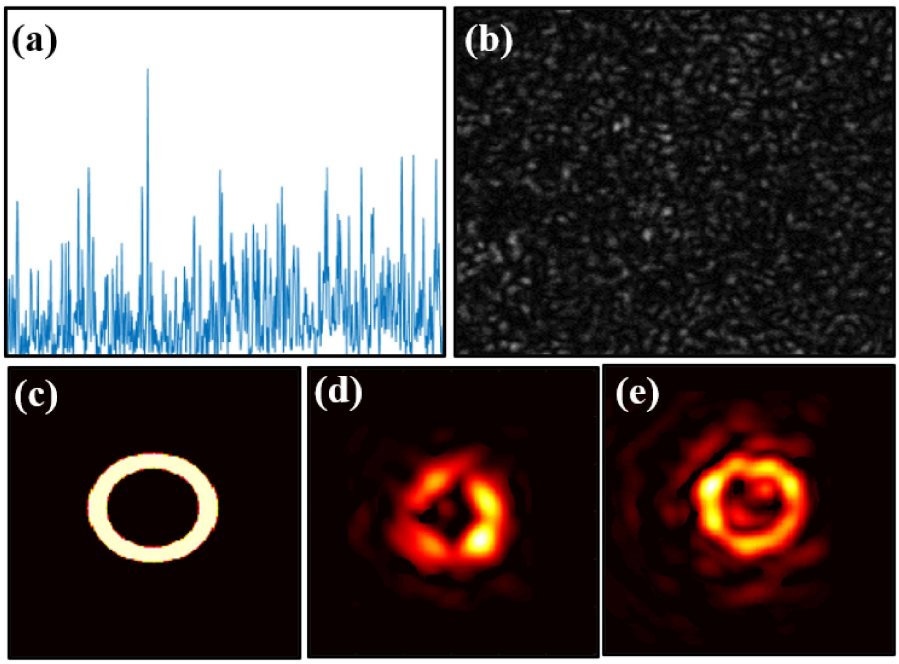

Fig. 5.5 (a) 1-D line profile for single-pixel used from object (Ring) experimental speckle (b) Experimentally recorded speckle without object information; (c) Original object; (d) and (e) indicate experimental and simulation reconstructed object transparency $\tau(\rho)$

Reduction algorithm is used to reduce the remaining noise from the retrieved image. For the quantitative analysis of the reconstructed results, we have calculated two parameters: visibility (v) and reconstruction efficiency η [27]. Visibility is defined as the extent to which the target reconstruction can be distinguished from the background noise and is measured as the proportion of the signal region's average intensity level to the background region's average intensity level in the reconstructed image. A global threshold technique is used to estimate the signal region. For annular ring, the calculated visibility values are 10.53 and 9.52 for simulation and experimental respectively. Similarly for second transparency i.e., sinusoidal grating, the visibility values for simulation and experiment are 8.70 and 8.46 respectively. Another important parameter for the quality evaluation

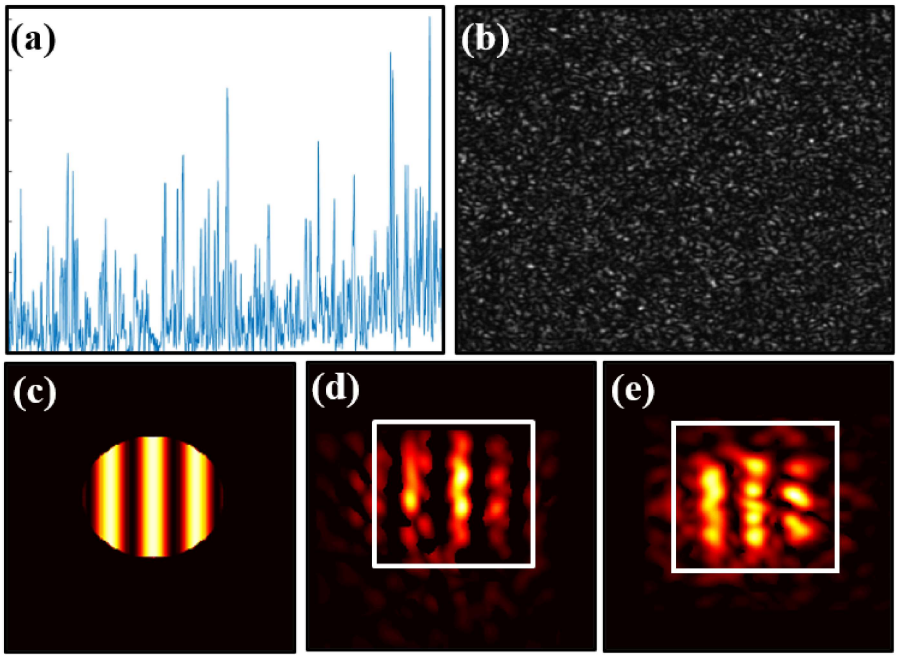

Fig. 5.6 (a) 1-D line profile for single-pixel used from object (Ring) experimental speckle (b) Experimentally recorded speckle without object information; (c) Original object; (d) and (e) indicate experimental and simulation reconstructed object transparency $\tau(\rho)$

is reconstruction efficiency η, which is defined as the ratio of measured power in the signal region of the retrieved image to the sum of the measured powers in the signal and background regions. The efficiency values for annular ring are 0.91 and 0.89, respectively for simulation and experiment. The calculated η values for sinusoidal grating are 0.89 and 0.88 for simulation and experiment, respectively.

Experimentally recorded random patterns for an annular ring are shown in Figs. 5.5 (a) and 5.5 (b). Fig. 5.5 (a) shows a 1D pattern detected by a single pixel at different spatial points for a binary transmittance function 'ring'. A 2D reference random field without transparency is shown in Fig. 5.5(b). The original object i.e., annular ring transparency used for reconstruction is shown in 5.5(c). Reconstruction of the transparency from the intensity correlation of these two fields is shown in Fig. 5.5(d). Reconstruction of the 'ring' from the simulated random fields is also demonstrated and shown in Fig. 5.5(e).

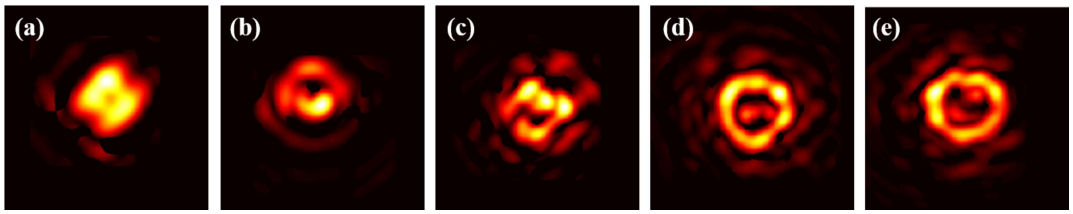

Fig. 5.7 Results for different sizes of Tuckey window used in the algorithm

We have also evaluated the reconstruction of a gradually changing transparency such as a sinusoidal function. The size of this transparency is restricted by an aperture of size 4.8 mm. Reconstruction of a sinusoidal grating transparency is shown in Fig. 5.6. Figs. 5.6 (a) and 5.6 (b) are 1D and 2D random fields. The original object, i.e., sinusoidal grating transparency used for reconstruction, is shown in 5.6(c), and reconstruction of the transparency is shown in Figs. 5.6 (d) and 5.6 (e) for experimental and simulated cases, respectively. The slight variation in experiment and simulation results arises due to experimental limitations such as limited size optics and limited size of recorded speckle patterns. The reconstruction quality further depends on factors like the correlation length of the source, i.e., illumination speckle size at the object plane, and also the number of speckle grains (independent patches) available at the recording plane for spatial averaging. The quality of retrieved results is effectively determined by the size of the Tuckey window used in the phase retrieval algorithm.

A 2D tuckey window is applied to the correlation function of intensity fluctuations in order to avoid the noisy region of the correlation. The higher frequency content of the intensity Fourier spectrum is influenced by the size of the Tuckey window used to filter the speckle autocorrelation function and, as a result, affects the object reconstruction. Reconstructed results are given in Fig. 5.7 for different sizes of Tuckey windows used in the process of phase retrieval algorithm. Fig. 5.7 (a-e) represents sizes of the Tuckey window 10,20,30,40,50 and 60 pixels respectively, from the correlation function where

an optimized size of the Tuckey window gives the best reconstructed result at a size of 60 pixels.

5.5 Ghost Polarimetry

Most of the GD and GI techniques that are currently in use have been centered on obtaining information about the characteristics of the object and not related with its polarization properties except in some recent investigations. Polarization plays a very important role in imaging techniques for obtaining information beyond what is revealed by their spectral and intensity distributions. Recently few polarization based techniques have been developed [124, 125]. In polarimetric ghost imaging setups, the reflective intensity of objects is decomposed into different polarization intensities. However, most of such schemes recover the polarization state for different polarization-sensitive objects based on Jones or Mueller matrix. In this section, we propose and demonstrate yet another approach for ghost polarimetry by evaluating the Stokes fluctuations from Stokes parameters of an object with an incident diagonally polarized beam. A conceptual representation of measuring Stokes parameters in Ghost diffraction is shown in Fig. 5.8. Four Stokes parameters are measured for different orientations of QWP and P. The first three Stokes parameters are measured by removing the QWP (or keeping at angle 0° and rotating the polarizer to the angles 0°,45°, and 90°. The final Stokes parameter S_3 is measured by keeping QWP at an angle 90° and setting the transmission axis of the polarizer to 45°. Using these Stokes parameters, a correlation between them is measured computationally. For an incident light beam, the fluctuations of Stokes parameters are given by the following,

$$\Delta S_n(r) = S_n(r) - \langle S_n(r) \rangle \tag{5.17}$$

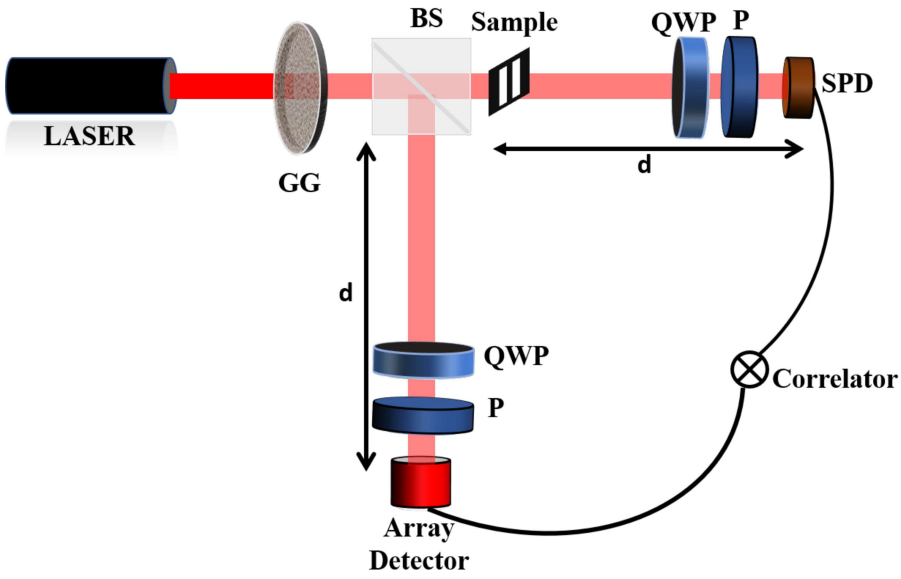

Fig. 5.8 Conceptual representation of measuring Stokes parameters in Ghost diffraction; GG: Ground glass, BS: Beam Splitter, SPD: Single Pixel Detector, QWP: Quarter wave plate, P: Polarizer

where $S_n(r)$ are the Stokes parameters at the observation plane with spatial point r and $n = 0,1,2,3$. A correlation between these Stokes parameters can be represented, A two-point correlation can be expressed as,

$$C_{nm}(r_1, r_2) = \langle \Delta S_n(r_1) \Delta S_m(r_2) \rangle \tag{5.18}$$

where $n, m = 0,1,2,3$. r_1 and r_2 are two spatial points at the observation plane, and $r_2 = r_1 + \Delta r$. A diagonally polarized light beam is incident on the object, and four Stokes parameters, i.e., S_0, S_1, S_2 and S_3 are measured. We use only one detector for the recording of Stokes parameters of object and reference in a similar way to the intensity random patterns shown in Fig. 5.3 but here for the Stokes parameters measurement. The Stokes fluctuations are calculated from two sets of Stokes parameters, one with the object information and the other without any object information. A two-point Stokes parameters correlation between the same Stokes parameters is measured, and C_{00}, C_{11}, C_{22}, and C_{33}

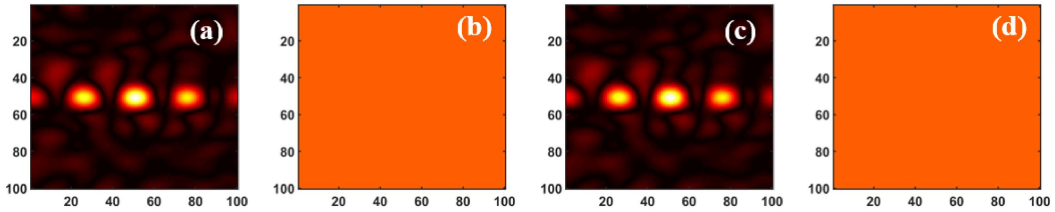

Fig. 5.9 Stokes fluctuations; (a-d) C_{00}, C_{11}, C_{22}, and C_{33}

are calculated. The elements of the Stokes fluctuation matrix can be given as [5, 53],

$$C_{nm}(r_1, r_2) = \langle S_n(r_1) S_m(r_2) \rangle - \langle S_n(r_1) \rangle \langle S_m(r_2) \rangle \tag{5.19}$$

By utilizing Eq. 5.18 and making a few combinations of Stokes fluctuations, generalized Stokes parameters are calculated. Two generalized Stokes parameters can be given as,

$$GS_0(r_1, r_2) = C_{00} + C_{22} + C_{11} + C_{33} \tag{5.20}$$

$$GS_2(r_1, r_2) = C_{00} + C_{22} - C_{11} - C_{33} \tag{5.21}$$

The Stokes fluctuations i.e. C_{00}, C_{11}, C_{22}, and C_{33} are given in Fig. 5.9. Two generalized Stokes parameters that survived for the case of the diagonally polarized incident beam, are shown in the first row of Fig. 5.10. The generalized Stokes parameters are fed to the same phase retrieval algorithm [220] as explained in section 5.2 and figure 5.2. Implementation of the phase retrieval algorithm with a few constraints is utilized for the full spatial polarimetric recovery and a reconstruction of object obtained with different polarization states is shown in the second row of Fig.5.10.

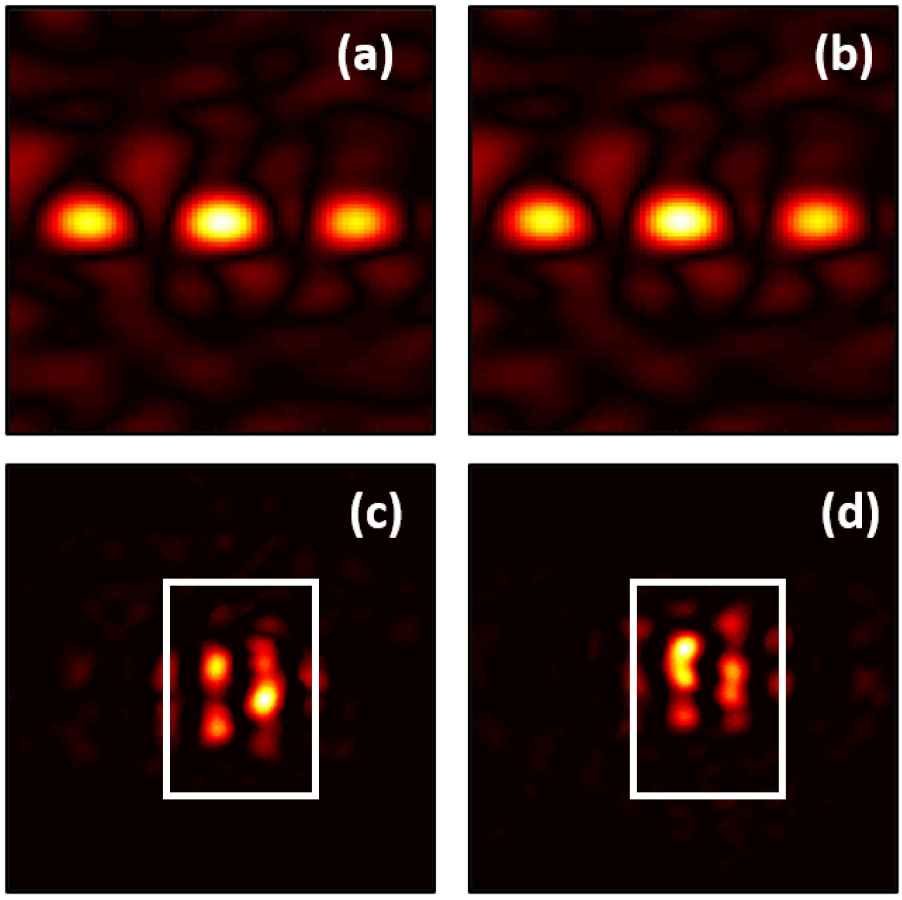

Fig. 5.10 Generalized Stokes parameters GS_0 (a), and GS_2 (b). Retrieved object results;(c) and (d) for two parallel strips corresponding to (a) and (b)

5.6 Conclusion

In conclusion, we have proposed and experimentally demonstrated a new ghost diffraction scheme by exploiting the correlation features of the spatially varying random fields. Based on the new strategy, the technique is capable of reconstructing the object by utilizing the spatial points in the random pattern. The novelty of the technique lies in the significant use of spatial averaging over temporal averaging as used in conventional ghost diffraction schemes. This leads to reconstruct the transparency with only two-time frozen random patterns. The simulation and experimental results are presented for two different objects. Moreover, we have proposed a technique for ghost diffraction in vectorial domain.

The technique uses generalized Stokes parameters derived from combinations of Stokes fluctuation and a phase retrieval algorithm as also explained in section 5.4. Simulation results are presented for an object “two parallel strips” with different polarization states. These methods open a wide range of applications in microscopy, polarization imaging, and encryption, etc.